Supplementary Information

Supplementary Figures

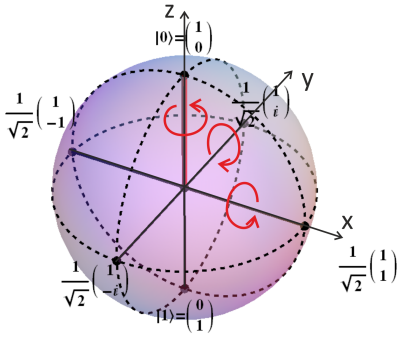

Supplementary Figure 1: **Bloch sphere.** Representation of the Bloch vector $|\psi_{ok}\rangle = \zeta|0\rangle + \xi|k\rangle$ on the Bloch sphere of the Hilbert sub-space spanned by the states $|0\rangle$ and $|k\rangle$ (where $k \in \{+, -\}$).

Supplementary Tables

Supplementary Table 1: **Convention of basis operators.** List of full set of nine basis operators building a suitable basis for the decomposition of the 3D process matrix χ and the reduced 2D process matrix $\chi^{(+-)}$ defined in Supplementary Equation (16).

E_m	Pauli operator	explicit expression	matrix representation	normalization factor α_m
E_1	$I_+ + I_-$	$\|+\rangle\langle+\| + \|-\rangle\langle-\|$	$\begin{pmatrix} 1 & 0 & 0 \\ 0 & 1 & 0 \\ 0 & 0 & 0 \end{pmatrix}$	$\sqrt{3/2}$
E_2	σ^x_{+-}	$\|+\rangle\langle-\| + \|-\rangle\langle+\|$	$\begin{pmatrix} 0 & 1 & 0 \\ 1 & 0 & 0 \\ 0 & 0 & 0 \end{pmatrix}$	$\sqrt{3/2}$
E_3	σ^y_{+-}	$-i\|+\rangle\langle-\| + i\|-\rangle\langle+\|$	$\begin{pmatrix} 0 & -i & 0 \\ i & 0 & 0 \\ 0 & 0 & 0 \end{pmatrix}$	$\sqrt{3/2}$
E_4	σ^z_{+-}	$\|+\rangle\langle+\| - \|-\rangle\langle-\|$	$\begin{pmatrix} 1 & 0 & 0 \\ 0 & -1 & 0 \\ 0 & 0 & 0 \end{pmatrix}$	$\sqrt{3/2}$
E_5	σ^x_{+0}	$\|+\rangle\langle0\| + \|0\rangle\langle+\|$	$\begin{pmatrix} 0 & 0 & 1 \\ 0 & 0 & 0 \\ 1 & 0 & 0 \end{pmatrix}$	$\sqrt{3/2}$
E_6	σ^y_{+0}	$-i\|+\rangle\langle0\| + i\|0\rangle\langle+\|$	$\begin{pmatrix} 0 & 0 & -i \\ 0 & 0 & 0 \\ i & 0 & 0 \end{pmatrix}$	$\sqrt{3/2}$
E_7	σ^x_{-0}	$\|-\rangle\langle0\| + \|0\rangle\langle-\|$	$\begin{pmatrix} 0 & 0 & 0 \\ 0 & 0 & 1 \\ 0 & 1 & 0 \end{pmatrix}$	$\sqrt{3/2}$
E_8	σ^y_{-0}	$-i\|-\rangle\langle0\| + i\|0\rangle\langle-\|$	$\begin{pmatrix} 0 & 0 & 0 \\ 0 & 0 & -i \\ 0 & i & 0 \end{pmatrix}$	$\sqrt{3/2}$
E_9	I_0	$\|0\rangle\langle0\|$	$\begin{pmatrix} 0 & 0 & 0 \\ 0 & 0 & 0 \\ 0 & 0 & 1 \end{pmatrix}$	$\sqrt{3}$

Supplementary Table 2: **Pulse sequence for quantum process tomography.** List of the full set of nine basis states employed for QPT in this work. In the third column EXC means state initialization into the $m_s = 0$ state by optical pumping via a ~ 4 μs long pulse of excitation light). The $(\tau)_{ijk}$ signify a microwave i-pulse of length τ on the j to k transition. DET means projective readout of the $m_s = 0$ population via ~ 300 ns of excitation light and simultaneous fluorescence detection.

Ψ_j	explicit expression	initialization	projective readout
Ψ_1	$\|+\rangle$	EXC + $\pi_{\bar{y}0+}$	π_{y0+} + DET
Ψ_2	$\|-\rangle$	EXC + $\pi_{\bar{y}0-}$	π_{y0-} + DET
Ψ_3	$\|0\rangle$	EXC	DET
Ψ_4	$\frac{1}{\sqrt{2}}(\|0\rangle + \|+\rangle)$	EXC + $\left(\frac{\pi}{2}\right)_{\bar{y}0+}$	$\left(\frac{\pi}{2}\right)_{y0+}$ + DET
Ψ_5	$\frac{1}{\sqrt{2}}(\|0\rangle + i\|+\rangle)$	EXC + $\left(\frac{\pi}{2}\right)_{\bar{x}0+}$	$\left(\frac{\pi}{2}\right)_{x0+}$ + DET
Ψ_6	$\frac{1}{\sqrt{2}}(\|0\rangle + \|-\rangle)$	EXC + $\left(\frac{\pi}{2}\right)_{\bar{y}0-}$	$\left(\frac{\pi}{2}\right)_{y0-}$ + DET
Ψ_7	$\frac{1}{\sqrt{2}}(\|0\rangle + i\|-\rangle)$	EXC + $\left(\frac{\pi}{2}\right)_{\bar{x}0-}$	$\left(\frac{\pi}{2}\right)_{x0-}$ + DET
Ψ_8	$\frac{1}{\sqrt{2}}(\|+\rangle + \|-\rangle)$	EXC + $\left(\frac{\pi}{2}\right)_{\bar{y}0+}$ + $\pi_{\bar{y}0-}$	π_{y0-} + $\left(\frac{\pi}{2}\right)_{y0+}$ + DET
Ψ_9	$\frac{1}{\sqrt{2}}(\|+\rangle + i\|-\rangle)$	EXC + $\left(\frac{\pi}{2}\right)_{\bar{y}0+}$ + $\pi_{\bar{x}0-}$	π_{x0-} + $\left(\frac{\pi}{2}\right)_{y0+}$ + DET

Supplementary Table 3: **Microwave pulse convention.** Definition of the rotation operators of the Bloch vector on the respective Hilbert sub-space spanned by either $|0\rangle$ and $|+\rangle$ or $|0\rangle$ and $|-\rangle$. The phase factor is acquired starting from the $|0\rangle$ state.

MW pulse phase	pulse type	state transformation	pulse type	state transformation
$\sin(\omega_{0\pm}t)$	$(\pi/2)_{x0+}$	$\begin{pmatrix} 1 & 0 & -i \\ 0 & \sqrt{2} & 0 \\ -i & 0 & 1 \end{pmatrix}/\sqrt{2}$	$(\pi/2)_{x0-}$	$\begin{pmatrix} \sqrt{2} & 0 & 0 \\ 0 & 1 & -i \\ 0 & -i & 1 \end{pmatrix}/\sqrt{2}$
$\sin(\omega_{0\pm}t + \pi)$	$(\pi/2)_{\bar{x}0+}$	$\begin{pmatrix} 1 & 0 & i \\ 0 & \sqrt{2} & 0 \\ i & 0 & 1 \end{pmatrix}/\sqrt{2}$	$(\pi/2)_{\bar{x}0-}$	$\begin{pmatrix} \sqrt{2} & 0 & 0 \\ 0 & 1 & i \\ 0 & i & 1 \end{pmatrix}/\sqrt{2}$
$\sin(\omega_{0\pm}t + \frac{\pi}{2})$	$(\pi/2)_{y0+}$	$\begin{pmatrix} 1 & 0 & 1 \\ 0 & \sqrt{2} & 0 \\ 1 & 0 & 1 \end{pmatrix}/\sqrt{2}$	$(\pi/2)_{y0-}$	$\begin{pmatrix} \sqrt{2} & 0 & 0 \\ 0 & 1 & 1 \\ 0 & 1 & 1 \end{pmatrix}/\sqrt{2}$
$\sin(\omega_{0\pm}t - \frac{\pi}{2})$	$(\pi/2)_{\bar{y}0+}$	$\begin{pmatrix} 1 & 0 & - \\ 0 & \sqrt{2} & 0 \\ -1 & 0 & 1 \end{pmatrix}/\sqrt{2}$	$(\pi/2)_{\bar{y}0-}$	$\begin{pmatrix} \sqrt{2} & 0 & 0 \\ 0 & 1 & -1 \\ 0 & -1 & 1 \end{pmatrix}/\sqrt{2}$

Supplementary Notes

Supplementary Note 1: Quantum process tomography

Quantum process tomography provides a means of determining the process matrix of an unknown quantum process acting on a quantum state [3]. It allows for the determination of the fidelity with which a specific quantum operation is performed experimentally in comparison to the theoretical, ideal process. Consider a general initial mixed quantum state

$$\rho^{\text{in}} = \sum_k p_k |k\rangle\langle k| \tag{1}$$

(where the states $|k\rangle \in \mathcal{H}^d$, $0 \leq p_k \leq 1$ and $\sum_k p_k = 1$). An arbitrary operation $\mathcal{E}$ acting on that state

$$\rho^{\text{in}} \longrightarrow \mathcal{E}(\rho^{\text{in}}) = \rho^{\text{out}} \tag{2}$$

can be described by a quantum process matrix χ_{mn} generating the final state

$$\rho^{\text{out}} = \mathcal{E}(\rho^{\text{in}}) = \sum_{mn} \chi_{mn} E_m \rho^{\text{in}} E_n^\dagger \tag{3}$$

where $\{E_m\} \in \mathcal{SU}(d)$ represent a full set of orthogonal basis operators. The fidelity of the quantum process is then given by the overlap between the experimentally performed transformation $\mathcal{E}$ and the theoretically ideal transformation U as

$$\mathcal{F}(\mathcal{E}, U) = \text{Tr}(\chi_{\text{exp}} \chi_{\text{theo}}) \tag{4}$$

with the experimental and theoretical representation of the process matrix χ_{exp} and χ_{theo}, respectively [1]. Since we reconstruct the fidelity of an intrinsically fault-tolerant quantum gate by means of standard QPT based on relatively vulnerable dynamical phase shifts, it is instructive to normalize the fidelity of the i-th quantum gate $\mathcal{F}_i$ obtained over standard QPT with respect to the fidelity of the QPT operation itself $\mathcal{F}_{\text{Id}}$ (i.e. an "empty" QPT run without quantum gate). Thus we obtain the relative fidelities

$$\widetilde{\mathcal{F}}_i(\mathcal{E}, U) = \frac{\mathcal{F}_i}{\mathcal{F}_{\text{Id}}} \tag{5}$$

as a sensible means for benchmarking the quantum gate performance achieved in this work.

Supplementary Note 2: Theoretical concept of the QPT procedure

Quantum process tomography is performed in d^4 runs, in each of which the system has to be initialized into a (quasi-)pure state $|\Psi_j\rangle \in \{|\Psi_1\rangle, |\Psi_2\rangle, ..., |\Psi_j\rangle\}$, where the d^2 states $|\Psi_j\rangle$ are chosen such that the corresponding density matrices $\rho_j = |\Psi_j\rangle\langle\Psi_j|$ form a basis for the space of matrices:

$$\rho = \sum_j q_j \rho_j = \sum_j q_j |\Psi_j\rangle\langle\Psi_j| \ . \tag{6}$$

Now, for each of the d^4 runs the unknown quantum process performs the transformation $\mathcal{E}$ on the full set of basis states ρ_j^{in} $(j = 1, ..., 9)$:

$$\rho_j^{\text{in}} \longrightarrow \mathcal{E}(\rho_j^{\text{in}}) = \rho^{\text{out}} \ . \tag{7}$$

In order to find an expression for the unknown transformation characterized by the process matrix χ_{mn} we decompose both $\mathcal{E}(\rho_j^{\text{in}})$ and $E_m \rho_j^{\text{in}} E_n^\dagger$ in the chosen state basis $\rho_k = |\Psi_k\rangle\langle\Psi_k|$:

$$\mathcal{E}(\rho_j^{\text{in}}) = \sum_k \lambda_{jk} \rho_k \ , \tag{8}$$

$$E_m \rho_j^{\text{in}} E_n^\dagger = \sum_k \beta_{jk}^{mn} \rho_k \ . \tag{9}$$

In general, the coefficients λ_{jk} and β_{jk}^{mn} are complex. While the β_{jk}^{mn} are to be determined theoretically on the basis of the formerly defined set of E_m and Ψ_j, the λ_{jk} are reconstructed from experimental results. We can construct the theoretical and experimental λ_{jk} by solving the linear system of equations for the observable

$$\mathcal{O}_{pj} = \langle\Psi_p|\mathcal{E}(\rho_j^{\text{in}})|\Psi_p\rangle = \sum_k \lambda_{jk} \langle\Psi_p|\rho_k|\Psi_p\rangle = \sum_k \lambda_{jk} |\langle\Psi_p|\Psi_k\rangle|^2 \tag{10}$$

corresponding to the d^2 projective measurements on the complete set of projection bases states Ψ_p. Analogously, we can determine the β_{jk}^{mn} by solving the respective linear system of equations

$$\langle\Psi_p|E_m\rho_j^{\text{in}}E_n^\dagger|\Psi_p\rangle = \sum_k \beta_{jk}^{mn}\langle\Psi_p|\rho_k|\Psi_p\rangle = \sum_k \beta_{jk}^{mn}|\langle\Psi_p|\Psi_k\rangle|^2 \ . \tag{11}$$

Combining both Supplementary Equation (8) and Supplementary Equation (9) we obtain

$$\mathcal{E}(\rho_j^{\text{in}}) = \sum_{mn}\chi_{mn}E_m\rho_j^{\text{in}}E_n^\dagger = \sum_{mn}\chi_{mn}\sum_k \beta_{jk}^{mn}\rho_k = \sum_k \lambda_{jk}\rho_k \ . \tag{12}$$

In fact, this relation holds for each ρ_k separately, so we may write

$$\sum_{mn}\chi_{mn}\beta_{jk}^{mn} = \lambda_{jk} \ . \tag{13}$$

If we now compute for every ρ_j the components κ_{jk}^{mn} as the generalized inverse of β_{jk}^{mn}

$$\sum_{mn}\chi_{mn}\underbrace{\sum_{jk}\beta_{jk}^{mn}\kappa_{jk}^{pq}}_{=\delta_{mp}\delta_{nq}} = \sum_{jk}\kappa_{jk}^{pq}\lambda_{jk} \tag{14}$$

we can find an explicit expression for the process matrix

$$\chi_{mn} = \sum_{jk}\kappa_{jk}^{mn}\lambda_{jk} \tag{15}$$

given in the basis of the generators E_m, E_n.

Supplementary Note 3: Theoretical and experimental choice of basis states and projection operators

For the quantum process tomography the basis operators E_k have to be chosen suitably. In a minimal setting these ought to be a full set of 8 generators of the $\mathcal{SU}(3)$, the so called the Gell-Mann matrices. These matrices need to be Hermitian, traceless ($\text{Tr}(E_i) = 0$) and satisfy $\text{Tr}(E_iE_j) = 2\delta_{ij}$. For the NV^- ground state triplet the suggested set is presented in Supplementary Table **1**. Here, we suggest a set of nine generators E_m of the $\mathcal{U}(3)$, as in this representation

the 4×4 process matrix $\chi^{(+-)}$ acting only in the Hilbert subspace $\mathcal{H}^2$ spanned by the computational states $|+\rangle$ and $|-\rangle$ can be immediately extracted from the full 9×9 process matrix χ as

$$\chi^{(+-)} = \left(Tr\{\widehat{\chi}^{(+-)}\} \right)^{-1} \cdot \widehat{\chi}^{(+-)} \ . \tag{16}$$

with

$$\widehat{\chi}^{(+-)} = \sum_{m,n=1}^{4} \mathrm{Tr}\{|e_m\rangle\langle e_n|\chi_{mn}\} \cdot |e_m\rangle\langle e_n| \tag{17}$$

where the $|e_m\rangle = (0, 0, ..., \delta_{im}, ..., 0) \in \mathbb{R}^4$ are unit vectors. The operators E_2 to E_8 are effectively Pauli operators acting only on a two-dimensional subspace of the total state space. The first and the ninth generator are chosen as (a suitable linear combination of) sub-space identity operators I_+, I_- and I_0.

The respective set of proposed basis states Ψ_j is given in Supplementary Table **2**. These states of the NV^- ground state triplet are to be prepared on the basis of microwave Rabi pulses applied to the $|0\rangle$ to $|+\rangle$ and the $|0\rangle$ to $|-\rangle$ transitions inducing rotations of the Bloch vectors on the two coupled Bloch sub-spheres spanned by the states $|0\rangle$ & $|+\rangle$ and $|0\rangle$ & $|-\rangle$, respectively (cf. Supplementary Figure **1**). An initial Bloch vector $|\psi\rangle$ is rotated to state $|\psi'\rangle$ upon application of a Rabi pulse R_{0k} following $|\psi'\rangle_{0k} = R_{0k}|\psi\rangle_{0k}$, where $|\psi\rangle_{0k} \in \mathcal{H}^2 = \{\zeta|0\rangle + \xi|k\rangle \mid \zeta, \xi \in \mathbb{C}\}$. Here, we want to employ the following convention for dynamic phase shifts induced by resonant microwave pulses of length $\tau = \beta/\Omega(t)$ on either of the $|0\rangle \leftrightarrow |+\rangle$ and the $|0\rangle \leftrightarrow |-\rangle$ transition:

$$R_{0+}(\alpha, \beta) = \begin{pmatrix} \cos(\beta/2) & 0 & -ie^{-i\alpha}\sin(\beta/2) \\ 0 & 1 & 0 \\ -ie^{i\alpha}\sin(\beta/2) & 0 & \cos(\beta/2) \end{pmatrix} \tag{18}$$

$$R_{0-}(\alpha, \beta) = \begin{pmatrix} 1 & 0 & 0 \\ 0 & \cos(\beta/2) & -e^{-i\alpha}\sin(\beta/2) \\ 0 & e^{i\alpha}\sin(\beta/2) & \cos(\beta/2) \end{pmatrix} \tag{19}$$

where β determines the rotation angle and α the rotation axis. An x pulse is considered a microwave sine pulse, an $\bar{\mathrm{x}}$ pulse has a relative phase shift of $\alpha = +\pi$, a y pulse a phase shift of $\alpha = +\frac{\pi}{2}$, and a $\bar{\mathrm{y}}$ pulse a phase shift of $\alpha = -\frac{\pi}{2}$. Explicit expressions for the rotation matrices of

the respective pulses are shown in Supplementary Table **3**. These sub-space rotation operations can be conveniently visualized on two coupled sub-space Bloch spheres. Supplementary Figure **1** shows the sub-space Bloch sphere spanned by the states $|0\rangle$ and $|+\rangle$. Bear in mind that as the two sub-space Bloch spheres are coupled, global phase factors arising due to rotations on a sub-space Bloch sphere are not negligible; indeed, they are relative phase factors on the respective generalized eight-dimensional Bloch sphere comprising both sub-space Bloch spheres.

The corresponding experimental preparation routines for the set of basis states ψ_j are proposed along with their corresponding projective readout sequences in the third and forth column of Supplementary Table **2**, respectively. In the case of the NV^- centre the state initialization is always performed by optical pumping into the $|0\rangle$ state followed by a suitable combination of microwave π and $\frac{\pi}{2}$ pulses. The projective readout follows the reverse scheme projecting the obtained state ρ^{out} back onto the $|0\rangle$ basis. This allows for the reconstructed of the decomposition of ρ^{out} in the basis of ρ_j.

Supplementary Note 4: Maximum likelihood estimation procedure

In order to extract the experimentally obtained process fidelity we fit the experimental data with a proper theoretical model by means of a maximum likelihood estimation (MLE) procedure. For this purpose the maximum likelihood function

$$\begin{aligned} f(\vec{q}) &= \sum_{j,p} \Big(\langle \Psi_p | \mathcal{E}(\rho_j^{\text{in}}) | \Psi_p \rangle - \sum_{m,n} \chi_{mn}(\vec{q}) \langle \Psi_p | E_m | \Psi_j \rangle \langle \Psi_j | E_n | \Psi_p \rangle \Big)^2 \\ &- \Lambda \Big(\sum_{m,n,r} \chi_{mn}(\vec{q}) \ \text{Tr}\big(\alpha_m \alpha_r \alpha_n E_m E_r E_n\big) - \delta_{r,1} \Big) \end{aligned} \tag{20}$$

is to be minimized, where Λ is a Lagrange multiplier and $\delta_{r,1}$ the Kronecker delta. The α_m are normalization factors (see Supplementary Table **1**) that allow for an direct extraction of the process matrix $\chi^{(+-)} \in \mathcal{H}^2$ (defined on the computational state space) from the fitted process

matrix $\chi^{(+-0)} \in \mathcal{H}^3$ (defined on the total system space) as stated in Supplementary Equation (16). The first term in Supplementary Equation (20) ensures hermiticity, while the second term sets the degree of positivity by means of a Lagrange mulitiplier Λ. Trace-preservation of the process matrix is satisfied per constructionem by the parametrized representation

$$\chi(\vec{q}) = \frac{Q^\dagger(\vec{q})Q(\vec{q})}{\mathrm{Tr}\{Q^\dagger(\vec{q})Q(\vec{q})\}} \tag{21}$$

or element-wise

$$\chi_{mn}(\vec{q}) = \left(\sum_{m',n'} \sum_{k} \delta_{m',n'} (Q_{km'})^* Q_{kn'} \right)^{-1} \cdot \left(\sum_{k} (Q_{km})^* Q_{kn} \right) \tag{22}$$

where the compelx valued matrix $Q(\vec{q})$ is a triangular matrix parametrized by a real valued vector $\vec{q}$ containing $d^4 - d^2$ elements. For the present case of $d = 3$ the $Q(\vec{q})$ matrix can be written as

$$Q(\vec{q}) = \begin{pmatrix} q_1 & 0 & 0 & 0 & 0 & 0 & 0 & 0 & 0 \\ q_2+iq_{10} & q_{18} & 0 & 0 & 0 & 0 & 0 & 0 & 0 \\ q_3+iq_{11} & q_{19}+iq_{26} & q_{33} & 0 & 0 & 0 & 0 & 0 & 0 \\ q_4+iq_{12} & q_{20}+iq_{27} & q_{34}+iq_{40} & q_{46} & 0 & 0 & 0 & 0 & 0 \\ q_5+iq_{13} & q_{21}+iq_{28} & q_{35}+iq_{41} & q_{47}+iq_{52} & q_{57} & 0 & 0 & 0 & 0 \\ q_6+iq_{14} & q_{22}+iq_{29} & q_{36}+iq_{42} & q_{48}+iq_{53} & q_{58}+iq_{62} & q_{66} & 0 & 0 & 0 \\ q_7+iq_{15} & q_{23}+iq_{30} & q_{37}+iq_{43} & q_{49}+iq_{54} & q_{59}+iq_{63} & q_{67}+iq_{70} & q_{73} & 0 & 0 \\ q_8+iq_{16} & q_{24}+iq_{31} & q_{38}+iq_{44} & q_{50}+iq_{55} & q_{60}+iq_{64} & q_{68}+iq_{71} & q_{74}+iq_{76} & q_{78} & 0 \\ q_9+iq_{17} & q_{25}+iq_{32} & q_{39}+iq_{45} & q_{51}+iq_{56} & q_{61}+iq_{65} & q_{69}+iq_{72} & q_{75}+iq_{77} & q_{79}+iq_{80} & q_{81} \end{pmatrix} \tag{23}$$

where $\vec{q} = (q_1, q_2, q_3, \ldots, q_{81})$ denotes the set of 81 fit parameters. In principle a suitable set of start values $\vec{q_0}$ for the iterative fit could be extracted from $\widetilde{\chi}^{\mathrm{exp}}$ obtained from the raw experimental data. Practically, however, in the case of $d > 2$ the reverse element-wise dependence of Supplementary Equation (22), i.e. Q_{kn} as a function of the $\widetilde{\chi}^{\mathrm{exp}}_{mn}$ is non-trivial:

$$Q_{kn}(\widetilde{\chi}^{\mathrm{exp}}_{mn}) =? \longrightarrow \vec{q_0}. \tag{24}$$

Once an explicit expression for Supplementary Equation (24) is found we might initialize the start value set to $\vec{q_0}$ based on $\widetilde{\chi}^{\mathrm{exp}}_{mn}$. For $d = 2$ an explicit solution for the start parameter set $\vec{q_0}(\widetilde{\chi}^{\mathrm{exp}}_{mn})$ exists (see [2]). To the best of our knowledge there has not been presented a closed-form expression for $d > 2$ in the literature until now. For our present case of $d = 3$ the relation in

Supplementary Equation (24) is highly non-trivial to compute. Thus, in this work we chose to find a start parameter set $\vec{q_0}$ as follows: First, we approximate the experimentally obtained $\widetilde{\chi}^{\mathrm{exp}}_{mn}$ by a positive definite version of that matrix through substitution of the (anyway small) negative diagonal entries in the diagonalized form of $\vec{q_0}(\widetilde{\chi}^{\mathrm{exp}}_{mn})$ by suitably small, but positive values) and subsequently performing a Cholesky decomposition. From the lower unit triangular matrix of the Cholesky decomposition we can extract a start value set $\vec{q_0}$ for the maximum likelihood estimation procedure.

Supplementary Note 5: Data Evaluation and error estimation for maximum likelihood fit of χ and $\mathcal{F}$

Due to the complex relation between the measured data and the final process matrix χ and the fidelity $\mathcal{F}$ the error calculation is non-trivial. Therefore, a Monte Carlo based error estimation method is employed here. The observables, i.e. the projective readout data from Supplementary Equation (10) are fitted by Gaussian distributions and the mean value $\overline{\mathcal{O}}_{pj}$ and standard deviation $\sigma_{\mathcal{O}_{pj}}$ of each observable fit is extracted. From a normally distributed set of Monte Carlo sampled observable values we obtain the corresponding distribution for the λ_{jk} coefficients and can extract mean value $\overline{\lambda}_{jk}$ and standard deviation $\sigma_{\lambda_{jk}}$ for each of the 81 λ_{jk}. From a normally distributed Monte Carlo sampled set of each of the 81 λ_{jk} coefficients we obtain a distribution for the χ^{raw}_{mn} elements and can extract 81 mean values $\overline{\chi}^{\mathrm{raw}}_{mn}$ and standard deviations $\sigma_{\chi^{\mathrm{raw}}_{mn}}$ as well as a mean process matrix

$$\overline{\chi}^{\mathrm{raw}} = \sum_{m,n=1}^{9} \mathrm{Tr}\{|e_m\rangle\langle e_n|\overline{\chi}^{\mathrm{raw}}_{mn}\} \cdot |e_m\rangle\langle e_n| \tag{25}$$

where the $|e_m\rangle = (0, 0, ..., \delta_{im}, ..., 0) \in \mathbb{R}^9$ are unit vectors.

Now the raw data process matrix $\overline{\chi}^{\mathrm{raw}}$ is subject to the MLE procedure described above (where the start parameter set is derived from the mean process matrix: $\chi(\vec{q_0}(\overline{\chi}^{\mathrm{raw}}))$) delivering

a fitted process matrix $\overline{\chi}^{\mathrm{MLE}}$. Ultimately, the total process fidelity of the i-th gate is computed with respect to the MLE fitted process matrix $\overline{\chi}_i^{\mathrm{MLE}}$ as

$$\mathcal{F}_i = \mathrm{Tr}(\overline{\chi_i}^{\mathrm{MLE}} \chi_i^{\mathrm{theo}}) \tag{26}$$

providing a reasonable figure of merit for the achieved performance of the quantum gate of interest.

In order to obtain an error estimation for this MLE fitted process matrix and the fidelity a large sample of normally distributed $\chi_{mn}^{\mathrm{raw\ MC}}$ with the previously determined standard deviation $\sigma_{\chi_{mn}^{\mathrm{raw}}}$ is subject to the maximum likelihood procedure as well resulting in a non-Gaussian distribution for the $\chi_{mn}^{\mathrm{MLE\ MC}}$. The error of the fidelity was derived from the (in general asymmetric) distribution of the fidelities computed from the respective Monte Carlo sets $\chi^{\mathrm{MLE\ MC}}$. The error bars given in the main article cover a 68.3% confidence interval around the fidelity values $\mathcal{F}_i$ and have to be seen as an upper bound error estimate, as the Monte Carlo sampled sets of $\chi_{mn}^{\mathrm{raw\ MC}}$ elements were uncorrelated. The obtained fidelity errors are in good agreement with the residua between the fidelities computed from the unfitted $\overline{\chi}^{\mathrm{raw}}$ and the fidelity computed from the fitted $\overline{\chi}^{\mathrm{MLE}}$.

In order to remove the fidelity bias originating from the infidelity of the characterizing quantum process tomography itself, the extracted fidelities of the i-th holonomic quantum gate $\widetilde{F}_i$ were obtained from a normalization of the respective total process fidelity F_i by the fidelity of the identity gate F_{ID}: $\widetilde{F}_i = \frac{F_i}{F_{\mathrm{ID}}}$.

Supplementary References

[1] Gilchrist, A., Langford, N. K. & Nielsen, M. A. Distance measures to compare real and ideal quantum processes. *Phys. Rev. A.*, **71**, 5, 062310 (2005).

[2] James, D. F. V., Kwiat, P. G., Munro, W. J. & White, A. G. Measurement of qubits. *Phys. Rev. A.*, **64**, 5, 052312 (2001).

[3] Nielsen,M. A. & Chuang,I. L. *Quantum Computation and Quantum Information.* (Cambridge University Press, Cambridge, 2005).